SPE-212663-MS

Numerical Investigation of Hybrid Smart Water and Foam Injections in Carbonate Reservoirs

Anas Mohammed Hassan, Department of Petroleum Engineering, Khalifa University of Science and Technology, UAE; Bennet N. Tackie-Otoo, Mohammed A. Ayoub, and Mysara E. Mohyaldinn, Department of Petroleum Engineering, Universiti Teknologi PETRONAS, Malaysia; Emad W. Al-Shalabi and Imad A. Adel, Department of Petroleum Engineering, Khalifa University of Science and Technology, UAE

 DOI 10.2118/212663-MS

This paper was prepared for presentation at the SPE Reservoir Characterisation and Simulation Conference and Exhibition held in Abu Dhabi, UAE, 24 - 26 January 2023.

Abstract

This contribution is a progressive effort to investigate the effect of the novel hybrid EOR method of Smart Water Assisted Foam (SWAF) technique on oil recovery from carbonates through numerical modeling. In this work, a core-scale model was utilized to provide an insight and a better understanding of the controlling mechanisms behind incremental oil recovery using a new hybrid EOR method consisting of a combination of smart water flooding and foam injection, termed as Smart Water Assisted Foam (SWAF) technology, particularly for carbonate reservoirs. A core-scale model encapsulating the physics of SWAF flooding was used to history-match experimental data and the model was further optimized utilizing the CMG simulator. For extracting the most value from this numerical investigation, a sensitivity analysis was performed to monitor the effect of influential parameters affecting oil recovery depending on the spectrum of the experimental data available. The objective functions used in the sensitivity analysis include minimizing the history-matching global error and maximizing the oil recovery profiles. Three sensitivity analysis approaches were used: Tornado-plot, SOBOL analysis, and MORRIS analysis. For generating the related proxy models, polynomial regression, and radial basis function (RBF) neural networks were investigated. Subsequently, the DECE-based and PSO-based optimization methods were employed to examine the effect of chemical design parameters such as smart water (Mg^{2+}), surfactant aqueous solution (SAS), and foam concentrations along with the liquid production rate on the oil recovery factor during SWAF-flooding.

Based on the numerical results, the experimental coreflooding data were accurately history-matched using the proposed model with a minimal error of 4.74% applying the PSO-based optimization method. Furthermore, in terms of the objective function prediction during the sensitivity analysis study, the comparative assessment of both proxy models on the verification plot reveals that the RBF neural network outperforms the polynomial regression. Consolidated findings from the three sensitivity analyses, i.e., the Tornado-plot, SOBOL, and MORRIS, outline three common parameters that significantly affect the oil recovery profiles that are liquid production rate (LigProdCon), foam (DTRAPW SAS2), and Mg^{2+} concentration (DTRAP Mg3) parameters. On the other hand, in terms of maximizing the oil recovery while

minimizing the usage of injected chemicals during SWAF flooding, the optimal solution via the PSO-based approach is superior (97.89%) to the DECE-based optimal solutions (92.47%). This work presents one of the few studies investigating the numerical modeling of the SWAF process and capturing its effects on oil recovery. The optimized core scale model can be further used as a base for building a field-scale model and designing a successful pilot project.

Introduction

The production stages of a traditional crude oil project are normally categorized into three stages. The reservoir's natural pressure influences crude oil production during the primary stage of recovery. The secondary stage involves injecting water or gas to maintain constant reservoir pressure (Suarez-Rivera *et al.,* 2002). Afterwards, an operator may pursue additional recovery during the tertiary stage, termed enhanced oil recovery (EOR). This stage can be very beneficial since the secondary stage can typically only recover about 30% of the crude oil in the reservoir, leaving behind roughly 70% of the oil initially in place (OIIP). Moreover, the International Energy Agency (IEA) forecasts that by 2040, the supply of crude oil will only contribute to about 30% of the world's energy demand (IEA, 2020 and 2021). Furthermore, the likelihood of discovering new oil and gas reserves has decreased due to concerns about climate change (Bai and Xu, 2014). As a result, mature reservoirs have greater significance for sustaining global oil production (Alvarado and Manrique, 2010). To assuage these concerns, EOR can prevent the decline of mature fields and increase the overall recovery rate.

With the further aging of oil reservoirs, the economic significance of carbonates reservoirs has grown massively since approximately 60% of the world's reserves are preserved in carbonates (Akbar *et al.,* 2000). Generally, gas injection is the preferred enhanced oil recovery method in carbonate rocks (Taber *et al.,* 1997; Lake *et al.,* 2014). However, this method faces issues such as the early breakthrough of gas through carbonate strata and the unfavorable mobility caused by low viscosity of N_2 and CO_2 gases (Masalmeh *et al.,* 2011; Yuncong *et al.,* 2014). This unwanted gas mobility in carbonate formations leads to weak volumetric sweep efficiency due to viscous fingering, gravity override, and channeling problems (Dullien *et al.,* 1989). The poor volumetric sweep efficiency during gas injection can be resolved through Foam Assisted Water Alternating Gas (FAWAG) injection. Foam flooding improves the volumetric sweep efficiency while diminishing the gas-oil ratio to enhance oil recovery (Aarra *et al.,* 2002; Blaker *et al.,* 2002; Masalmeh *et al.,* 2011; Masalmeh, 2012; Tunio *et al.,* 2012). Nonetheless, there is the critical issue of foam-oil interaction during FAWAG (Foam Assisted Water Alternating Gas) injections, where the crude oil phase destroys the generated foam (Schramm and Novosad, 1992; Denkov, 2004; Garrett, 2017). Several researchers reported that the crude oil's composition destabilizes the foam (Kuhlman, 1990; Schramm *et al.,* 1993; Dalland *et al.,* 1994; Vikingstad *et al.,* 2005; Simjoo *et al.,* 2013). Based on laboratory and field pilot data, smart water injection has been observed to influence carbonate rock's wettability significantly, improving the recovery factor increment of carbonate formations (Hiorth *et al*., 2008 and 2010; Al-Shalabi *et al.,* 2014 and 2016). Thus, the Smart-Water Assisted Foam (SWAF) flooding has been introduced as an effective strategy for water film and foam lamellae stabilization (Hassan *et al.,* 2020a, 2020b, 2020c, 2022a, and 2022d).

The techniques of smart water and foam injections are well-established EOR methods that can increase oil recovery of residual and remaining oil from a carbonate rock above the waterflooding levels (Ali *et al.,* 1985; Kuhlman, 1990; Denkov, 2004; Studart *et al.,* 2007; Espinosa *et al.,* 2010; Xue *et al.,* 2016; Garrett, 2017). The hybrid combination of smart water and foam injection (i.e., SWAF) floodings is an emerging EOR technique, proven to be amply effective, especially in carbonates, as laboratory experiments reveal (Hassan *et al.,* 2019, 2021, 2022b, and 2022c). The emergent SWAF technology has recently attracted much interest owing to its remarkable synergistic potential for EOR application. The SWAF technique is specifically effective in carbonates as they are mixed-to-oil wet, in which the smart water (SW) can change the rock's wettability towards a more water-wetting state (Hirasaki, 1991; Hiorth *et al.,* 2008; Hassan *et al.,* 2020b), and stabilize the foam lamellae (Hassan *et al.,* 2022c). Furthermore, the surfactant aqueous solution (SAS) can diminish the interfacial tension (IFT) (Morrow, 1991), which altogether results in an increased recovery factor (i.e., up to 92% OIIP) (Hassan *et al.,* 2021, 2022a, 2022c, and 2022d). The SWAF's smart water (SW-solution) design induces a so-called dual-enhancement effect on oil displacement by affecting the fluid-rock and the fluid-fluid interactions. The fluid-rock interactions are improved through surface charge alteration at the fluid-rock interface, resulting in wettability alteration of reservoir rock towards stronger water-wetness (Hiorth *et al.*, 2010). The fluid-fluid interactions are affected via SW-solution designs that create a reduction in the shielding effect of the electrical double layer (EDL) (Weller and Slater, 2012; Xie *et al.,* 2019), achieving foam film stabilization (Lunkenheimer and Malysa, 2003).

The injection scheme of the SWAF process, as shown in Figure 1, is divided into two stages. The leading stage consists of SW-solution injections for altering the reservoir rock wettability towards a more water-wet condition via improved water film stability and simultaneous foam lamellae stability enhancement through foam generation during the second stage. Subsequently, the second stage involves injecting SAS alternating gas (SAG) solutions to decrease the interfacial tension (IFT) between oil and water phases and enhance oil displacement efficacy. A substantial potential of incremental oil production via SWAF flooding (up to 92% OIIP) is seen during the coreflood experiments, as shown in Figure 2, which can be a potential candidate for the remaining oil production using SWAF floods.

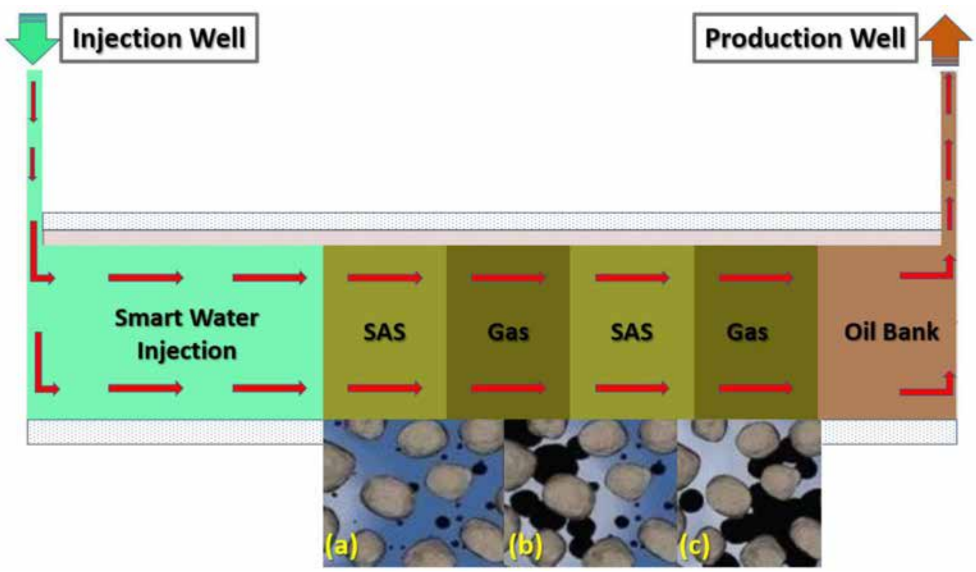

Figure 1—Schematic of SWAF starting with smart water as a secondary stage, followed by SAG (SAS Alternating Gas) flooding as a tertiary mode. (a) SWAF solutions in the occurrence of oil, (b) oil reacts to SWAF solutions, and (c) oil separates from the calcite rock and gets produced (Hassan *et al.,* 2022a).

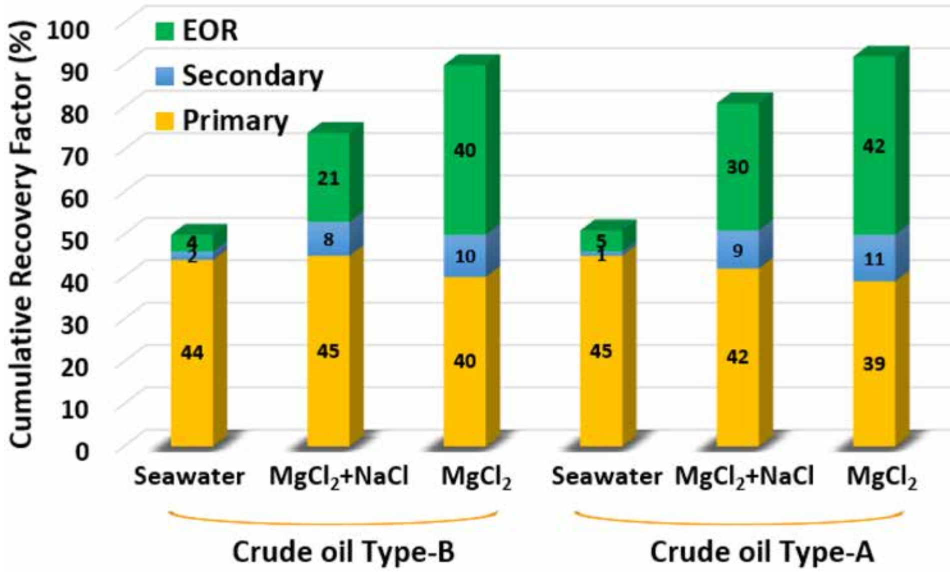

Figure 2—SWAF-injection scenarios: the coreflood experiment results show the effect of crude oil types (A and B) with various smart water solutions (i.e., 3,500 ppm) and at surfactant concentrations of 1000 ppm in SWAF-based EOR injection scenarios (Hassan *et al*., 2022a).

Thus, this contribution is a progressive effort to investigate the novel hybrid EOR method of Smart Water Assisted Foam (SWAF) technique through a numerical modeling perspective. Previous works have focused on coreflood laboratory evaluation, while this paper presents a numerical investigation at the core-scale for evaluating underlying recovery mechanisms, SWAF-oil interactions, and SWAF optimization for further implementation. This work utilizes a core-scale CMG-model to gather insights and better understand the mechanisms behind incremental oil recovery via the new hybrid EOR method of SWAF flooding, particularly for carbonate reservoirs. The developed CMG model is further applied for performing sensitivity analysis of several influential parameters, the history matching of the relative permeability curve and its interpolation parameters, and the optimization of SWAF flooding design. The objective functions of sensitivity analysis, history-matching, and optimization processes include global error reduction used to calibrate the simulation model through the experimental coreflood data and maximizing the recovery factor. Hence, this study seeks to expedite successful field applications of SWAF technology in carbonate reservoirs by thoroughly understanding crude oil/brine/rock (COBR) interactions at reservoir conditions (i.e., 80°C).

Methodology

In this study, the Computer Modeling Group (CMG) simulator was utilized for the core-scale numerical simulations. Figure 3 presents the methodical flowchart of this investigation. The CMG simulation tools were eventually applied in sequential stages to derive the optimal SWAF solution. At the onset, we determined the base case solution through an advanced processes reservoir simulator tool. Based on the experimental laboratory data, the Cartesian grid was built to mimic the core settings, and then the rock and fluid properties were specified. Subsequently, the PVT (pressure, volume, and temperature) table was prepared with rock-fluid data, and the initial reservoir conditions were considered in terms of pressure, saturation, and temperature. Then, the advanced processes reservoir simulation model was run to acquire the base case solution. In addition, to improve the base case results obtained from the advanced processes reservoir simulator, we performed a sensitivity analysis, history matching, and optimization studies using the optimization software described in the subsequent sections.

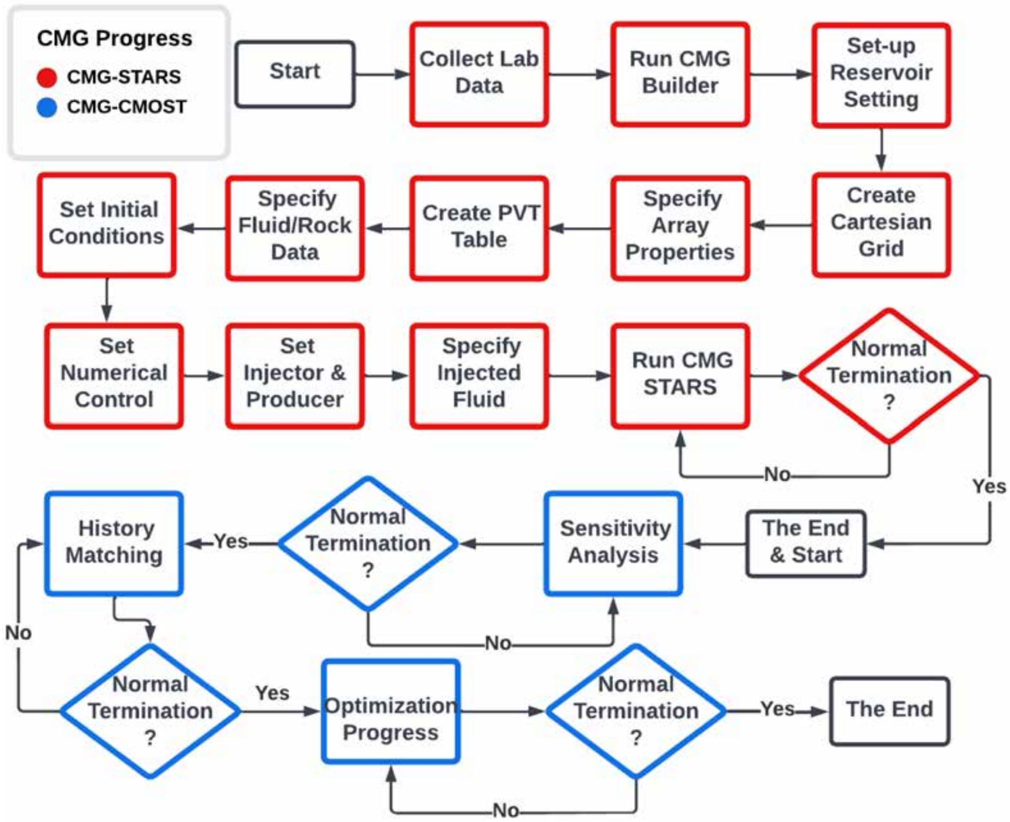

Figure 3—Flowchart for the numerical approach using CMG-simulator to advance the SWAF flooding process at a core-scale.

The Advanced Processes Reservoir Simulation Tool.

The advanced processes reservoir simulator (i.e., Steam and Thermal) is an adroit simulation and modeling tool that can recreate complex and advanced recovery processes such as gas, solvents, air, and chemicals injections (Zhang *et al.,* 2019; Kumar and Mandal, 2020). The advanced processes reservoir simulator is categorized by a finite difference numerical simulator, which can solve a sequence of conservation equations, including the material balance, flow, chemical processes, heat exchange, and phase equilibrium equations. The primary governing equations are associated with mass and energy conservation for the elementary volume (i.e., the region of interest), where the tuning for each component in the volume is related to the inflowing and outflowing of the injected fluids in the region of interest (i.e., core-sample) (Liu and Chen, 2018).

Apart from the basic conservation equations, the advanced processes reservoir simulator employs many relationships, and the key association is Corey's correlation. This correlation aims to construct relative permeability curves, which summarize the data on fluid-rock interactions. Due to the aqueous phase undergoing changes in the physicochemical properties impacted by the injection chemical (e.g., SWAF) solution, various fluid flow behaviors are interpreted by the advanced processes reservoir simulator via relative permeability curves interpolations (CMG, 2019). Corey's correlations are given by (Corey, 1977):

$$\mathbf{K_{rw}} = \mathbf{K_{rwiro}}\left(\frac{\mathbf{S_w} - \mathbf{S_{wcrit}}}{1.0 - \mathbf{S_{wcrit}} - \mathbf{S_{oirw}}}\right)^{\mathbf{N_w}}, \tag{1}$$

$$\mathbf{K_{row}} = \mathbf{K_{rocw}}\left(\frac{\mathbf{S_o} - \mathbf{S_{orw}}}{1.0 - \mathbf{S_{wcon}} - \mathbf{S_{orw}}}\right)^{\mathbf{N_{ow}}}, \tag{2}$$

$$\mathbf{K_{rog}} = \mathbf{K_{rogcg}}\left(\frac{\mathbf{S_l} - \mathbf{S_{org}} - \mathbf{S_{wcon}}}{1.0 - \mathbf{S_{gcon}} - \mathbf{S_{org}} - \mathbf{S_{wcon}}}\right)^{\mathbf{N_{og}}}, \tag{3}$$

$$K_{rg} = K_{rgcl}\left(\frac{S_g - S_{gcrit}}{1.0 - S_{gcrit} - S_{oirg} - S_{wcon}}\right)^{N_g}, \tag{4}$$

where K_{rw} is the water phase relative permeability for the water-oil table, K_{row} is the oil phase relative permeability for the water-oil table, K_{rog} is the liquid phase relative permeability for the liquid-oil table, K_{rg} is the gas phase relative permeability for the liquid-gas table, S_{wcon} is the connate water saturation, S_{wcrit} is the critical water saturation, S_{oirw} is the irreducible oil saturation for the water-oil table, S_{orw} is the residual oil saturation for the water-oil table, S_{oirg} is the irreducible oil saturation for the liquid-gas table, S_{org} is the residual oil saturation for the liquid gas table, S_{gcon} is the connate gas saturation, S_{gcrit} is the critical gas saturation, K_{rocw} is K_{ro} at connate water saturation, K_{rwiro} is K_{rw} at irreducible oil saturation, K_{rgcl} is K_{rg} at connate liquid saturation, K_{rogcg} is K_{rog} at connate gas saturation, N_w is the exponent for calculating K_{rw} from K_{rwiro}, N_{ow} is the exponent for calculating K_{row} from K_{rocw}, N_{og} is the exponent for calculating K_{rog} from K_{rogcg}, and N_g is the exponent for calculating K_{rg} from K_{rgcl}.

Equations (1) and (2) are used for the generation of the water-oil relative permeability table, and Equations (3) and (4) are used for the generation of the liquid-gas relative permeability table. The advanced processes reservoir simulator uses an interpolation of relative permeability curves for different flow behaviors of fluids that occur due to changes in the physicochemical properties of the aqueous phase caused by the presence of surfactant, polymer, and alkali. Typically, the relative permeability data is interpolated between two sets (or more), A and B, corresponding to high and ultralow IFT relative permeability curves, respectively (Cheng *et al.*, 2019). The values of the dimensionless interpolation parameters, with values varying between 0 and 1, are related to the capillary number (N_c) as follows (Hakiki *et al.,* 2015):

$$\text{ratw} = \frac{\log_{10}(N_c) - \text{DTRAPWA}}{\text{DTRAPWB} - \text{DTRAPWA}}, \tag{5}$$

$$\text{ratn} = \frac{\log_{10}(N_c) - \text{DTRAPNA}}{\text{DTRAPNB} - \text{DTRAPNA}}, \tag{6}$$

where DTRAPWA and DTRAPNA are interpolation parameters representing a low capillary number for high IFT values and a high capillary number for ultralow IFT values for the wetting phase, respectively. DTRAPNA and DTRAPNB are similar interpolation terms for the non-wetting phase. Thus, using one relative permeability dataset for high IFT values in the case of waterflooding and another relative permeability dataset for ultralow IFT values in the case of surfactant flooding. The relative permeability for intermediate IFT values is interpolated and used while running the simulation.

Model Description.. The SWAF-based EOR process was studied and investigated in the laboratory through core-flooding experiments. The laboratory investigation on SWAF flooding was conducted by linear and radial coreflood experiments at the reservoir temperature of 80°C (Hassan *et al*., 2022a and 2022d). A 1-D advanced processes reservoir simulation model was applied to simulate the coreflooding laboratory experiments. Given that the fluid flow in the core is more dominant in the axial direction compared to the radial direction, this 1-D model was chosen to simulate the flow of fluids in the axial direction of the core. The core sample, the fluids injected in the core, and the flow of fluids via the porous media of the core were all accurately represented in the core-model. The precision of these data indicates the closeness of the proposed 1-D model that matches the real coreflooding experiment.

The 1-D core-model was set horizontally to mimic the experimental setup with 200 grid blocks (200 × 1 × 1) based on grid sensitivity analysis study. The core sample's length and diameter of 7.6 cm and 3.82 cm respectively were captured in the model. Accordingly, the rock parameters, including permeability and porosity, were imitated, and assumed to be homogeneous for all grid-blocks based on the measured value of our chosen core sample (i.e., Indiana limestone, ILS). Regarding fluid properties, the different fluid parameters considered in the simulation model include the density and viscosity of the aqueous phase and the oleic phase. Table 1 summarizes the various input parameters for the model. Finally, one injector well and one producer well were included in the core-scale model. The positions of the oil producer and water injector wells are shown in Figure 4.

Table 1—Summary of fluid and rock petrophysical data for the carbonate core (i.e., Indiana Limestone, ILS) model used in the advanced processes reservoir simulator

Rock Properties	Value	Fluid Properties	Value
Gridblock Number	200	Water Viscosity (cP)	1.00311
Core Model Dimensions (cm)	7.6 × 3.385 × 3.385	Water Density (g/cm^3)	0.974
Gridblock Dimensions (cm)	0.038 × 3.385 × 3.385	Stock Tank Oil Gravity (API)	28
Permeability Kx, Ky, Kz (mD)	111.55	Oil Viscosity (cP)	2.23
Porosity Φ (%)	20	Oil Density (g/cm^3)	0.8694
Reservoir Pressure (psi)	2300	Initial Oil Saturation	0.52
Reservoir Temperature (°C)	80	Initial Water Saturation	0.48

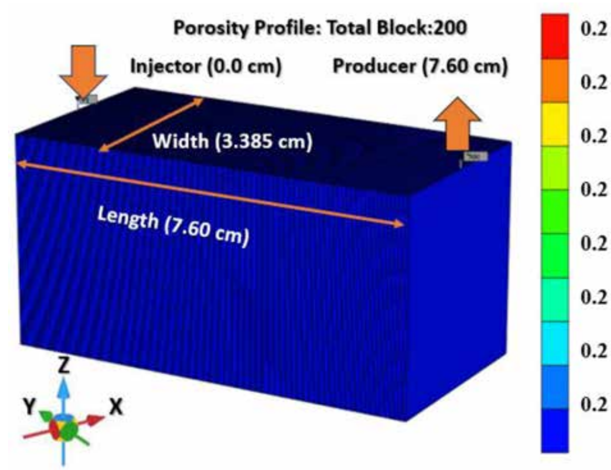

Figure 4—Porosity map for the core model where rock porosities were measured in the range of 20% showing similar contour maps.

Optimization Software Simulation.

The optimization software performed a sensitivity analysis, history matching, and optimization studies. The main goal of using the optimization software is to enhance the base case datasets (i.e., consisting of measured and assumed values), which is attained from the advanced processes reservoir simulator. For SWAF-based EOR flooding procedures, numerous parameters such as oil and water saturations (S_o and S_w), relative permeability, and chemical volume (i.e., the concentration of Mg and SAS) must be considered. Because the chemical cost constitutes a significant investment for this type of SWAF-based EOR project, the parameters mentioned above are essential to reflect the overall chemical consumption volume.

Sensitivity Analysis.. A sensitivity analysis was performed using the optimization software to understand how the various input parameters to the simulation models impact the simulation results (to determine various parameters with much influence on, e.g., the production profile). This is intended to improve the history matching and optimization processes (Zainal *et al.,* 2008; Douarche *et al.,* 2014). The sensitivity analysis started with 20 different parameters, as listed in Table 2. These parameters were evaluated to determine their effects on minimizing the global error and maximizing the oil recovery profiles reflected in the base case results.

Table 2—Defined baseline (default) values of the selected simulation inputs

Parameter Name	Default Value	Parameter Name	Default Value
DTRAPW_Foam1	0.0001	LiqProdCon	0.2
DTRAPW_Foam2	0.01	NG	2
DTRAPW_SAS1	−7	NOG	2
DTRAPW_SAS2	−3	Perm H	107.234
DTRAP_Mg1	0.00241013	PermV	107.234
DTRAP_Mg2	0.00128788	Porosity	0.187304
DTRAP_Mg3	0.000165641	SGCRIT	0.05
INJBHPCon	27579.028	SORG	0.1
KRGCL	0.8	S_O	0.670045
KROCW	1	S_W	0.329955

Initially, the sensitivity analysis was performed using the response surface methodology (RSM) (Zerpa *et al.,* 2007). The correlations among input parameters and objective functions are investigated via RSM. The central concept behind RSM is constructing a proxy model for replicating the original, sophisticated reservoir simulation model using a series of designed experiments. Polynomial regression and a neutral network with the radial basis function (RBF) were explored as two types of proxy models. The polynomial regression (i.e., in linear or quadratic forms) approach, which is the most frequently used proxy model, is defined as follows:

$$y = a_o + \sum_{j=1}^{k} a_j x_j + \sum_{j=1}^{k} a_{jj} x_j^2 + \sum_{i<j} \sum_{j=2}^{k} a_{ij} x_i x_j , \tag{7}$$

where a_o denotes the intercept, a_1, a_2… … .a_k denote the coefficients of the linear terms, a_{jj} stand for the quadratic terms coefficients, and a_{ij} denote cross (interaction) terms coefficients.

A radial basis function (RBF) neural network is a radial basis function (RBF) of a single-layer network with source nodes as an input layer, nonlinear processing units as a single hidden layer, and linear weights as an output layer. The input-output mapping executed via an RBF network can be defined as below:

$$\tilde{y}(x_p) = w_o + \sum_{i=1}^{M} w_i \varphi(x_i x_p) , \tag{8}$$

where $\varphi(x_i x_p)$, x_i, x_p and $\tilde{y}(x_p)$ denote the N-dimensional parameter space, while M denotes the training data size.

History Matching Study.. The history matching process is an optimization process with the objective function of minimizing the error between experimental and simulation data (i.e., global error percentage). The optimization software was used to perform the history matching of the simulation model, and 500 models were simulated with various combinations of the parameter values initially assumed for the base model. The different values of the parameters were generated by CMG's proprietary optimizer: Particle swarm optimization (PSO) and Designed Exploration and Controlled Evolution (DECE). The model with the least deviation between the simulated and the experimental results was regarded as the validated model. The various dynamic curves from the coreflood are compared to those obtained from the simulation, as shown in Figure 5 for history matching using the PSO approach.

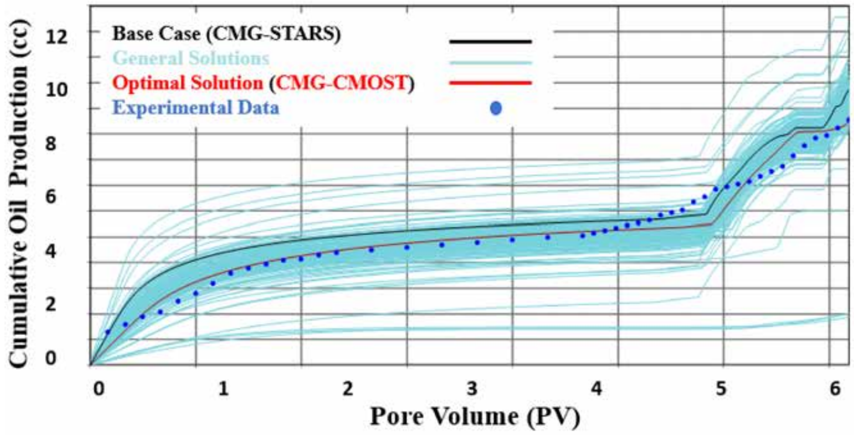

Figure 5—History matching results by Particle Swarm Optimization (PSO) approach.

Optimization Process.. After the history matching stage, CMG's proprietary optimizer PSO and DECE were used in the optimization process. The PSO is the most frequently used method in the optimization process. The PSO is a population-based stochastic optimization method developed by gaining inspiration from the social behavior of bird flocking and fish schooling (AlSofi and Blunt, 2011; Alkhatib and King, 2014). The objective function of the optimization process is to maximize the oil recovery factor. The primary operators in the PSO are the velocity and position updates. The following five steps summarize the basic algorithm of the PSO (CMG, 2019):

1. Swarm Initialization from the solution space.
2. Evaluating the appropriateness of every particle.
3. Individual updating and global bests.
4. Velocity and position updating of every particle.
5. Move to step 2 and replicate the step until the termination condition is reached, as shown in Figure 3.

Results and Discussion

The advanced processes reservoir simulator was utilized for simulating the coreflood experiment with SWAF slugs involving smart water and SAG (i.e., SAS alternating Gas), as depicted in Figure 6a (Hassan *et al.,* 2022a and 2022d). A substantial potential of incremental oil production via SWAF flood (up to 92% OIIP) is seen during the coreflood experiments, as shown in Figure 6b. Further, the advanced processes reservoir simulator was used for history matching the coreflood oil recovery data and to provide insight into the controlling relative permeability curves and related interpolation parameters. Before starting the SWAF flooding sequence, the core-model was initialized with the selected crude oil in each one of the grids. Subsequently, the core-sample model was flooded in sequence with formation water (i.e., FW, 35000 ppm), smart water ($MgCl_2$, 3500 ppm), and SAS Alternating Gas slugs (Figure 6a). Finally, the oil recovered from the production well was plotted as presented in Figure 6b. Comparing the coreflooding experimental oil recovery data (i.e., using scenario 1) to the simulation oil recovery results, which is the base case, shows a clear mismatch of the simulation model results with the experimental results, apparent from Figure 6b.

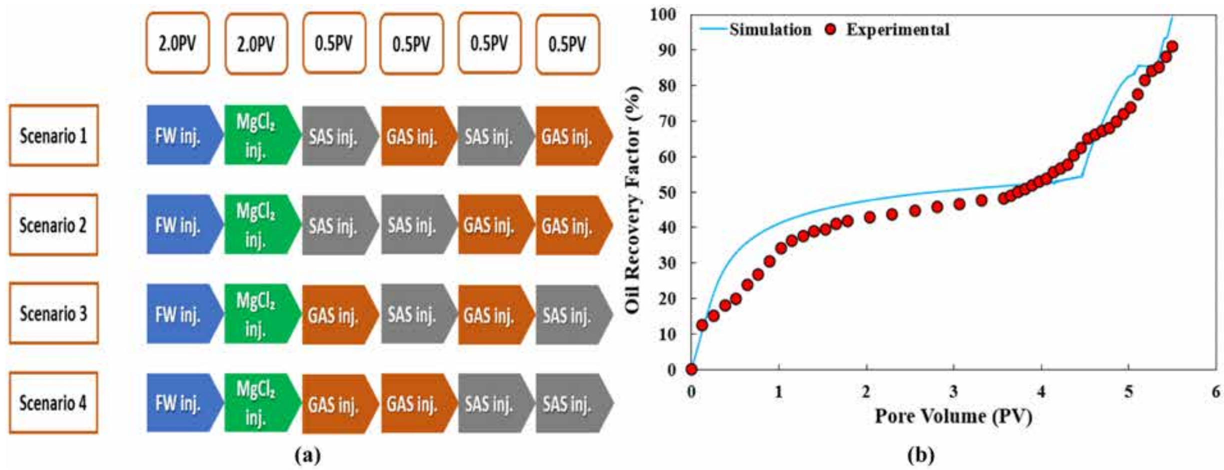

Figure 6—SWAF injection scenarios & Oil recovery production; (a) SWAF injection scenarios ($MgCl_2$ SAS+GAS with oil Type-A) to investigate the effect of slug size on oil recovery (Hassan *et al.,* 2022a and 2022d), and (b) Oil recovery factor (%) vs. injected Pore Volumes (PV) from simulation (i.e., base case model) and coreflooding experimental (i.e., using scenario 1) results.

Sensitivity Analysis.

The first primary task carried out using the optimization software simulator is the sensitivity analysis. In this task, we attempt to understand how the various inputs to the simulation model impact the simulation results (i.e., to minimize the history matching error and maximize the oil recovery profile). For this evaluation, 20 input parameters were selected and defined in the optimization software input parameters, as previously listed in Table 2. In the optimization software, the proxy modeling aids in defining the sensitivity of each effect on the simulation results (e.g., oil recovery profiles). The proxy model's utility also includes generating further quick predictions with no additional simulation (i.e., reducing the computational cost). The proxy models are also useful in certain proxy-based optimization algorithms for rapidly finding an optimal solution (Horowitz *et al.,* 2010).

Nevertheless, the proposed proxy model must be verified. Figures 7a and 7b depict the outcome of the verification plots for the polynomial and radial basis function (RBF) neural network proxy models, respectively. The model verification plot compares the actual response to the anticipated response for each training and verification run to indicate how well the data points fit the model. The error for each point is the distance from that point to the 45-degree line. Comparing these proxy models on the verification plot reveals that the RBF neural network outperforms the polynomial regression in predicting the objective function. This RBF proxy model was further utilized for the history matching and the optimization processes, as shown in Appendices A and B (Figures A-1 and B-1).

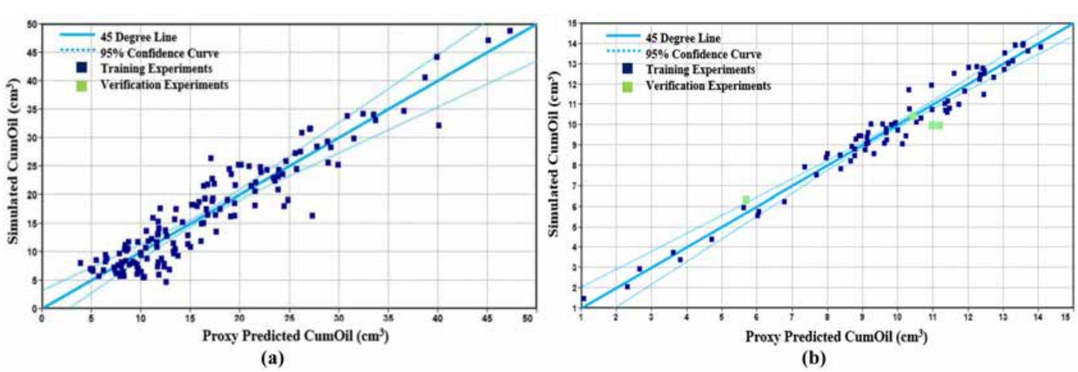

Figure 7—The verification plot for (a) polynomial regression proxy mode, and (b) radial basis function (RBF) neural network proxy mode.

A sensitivity analysis was performed to assess input parameters' influence on cumulative oil production using the one parameter at a time (OPAAT) approach (i.e., conventional approach). This approach aims to determine each parameter's influence by altering only one parameter at a time. Figure 8a depicts the outcome of this analysis as a Tornado-plot, according to which the liquid production concentration rate (i.e., LiqProdCon), oil and water saturations, porosity, and chemical concentration (i.e., Mg^{2+} and SAS) have the greatest impact on the oil recovery profiles. Furthermore, the sensitivity analysis suggests that the optimal chemical injection rate for the SWAF-based EOR flooding scenario requires further modification to increase sweep efficiency.

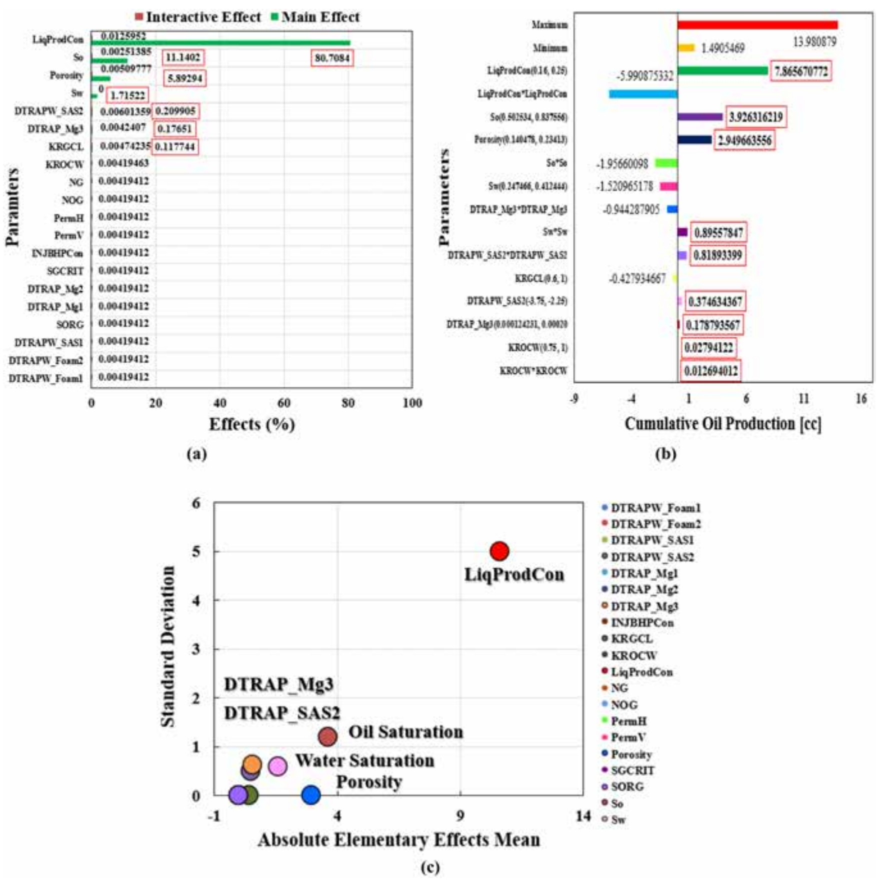

Figure 8—Sensitivity analysis results showing the effect of various parameters on the cumulative oil production using (a) The Tornado-plot, (b) The SBOL method, and (c) The MORRIS method.

In addition, the sensitivity analysis results were also presented in the SOBOL and MORRIS methods. The SOBOL and MORRIS are two variance-based sensitivity analysis procedures that are more recent (Garcia *et al.,* 2019). These methods aggregate each parameter's effects into a core effect and an interaction effect while performing the sensitivity analysis throughout the whole input area and identifying the non-linear responses (i.e., oil and gas reservoir responses are largely nonlinear). Therefore, this renders the analysis process more sophisticated and minimizes the number of runs. The SOBOL variance-based sensitivity analysis approach was used to analyze the results, as shown in Figure 8b. According to the SOBOL sensitivity analysis plot, the most influential parameters that have a positive impact on the oil recovery profiles during SWAF-based EOR are the liquid production rate (LigProdCon of 7.8 cc), oil saturation (S_o of 3.9 cc), porosity (at 2.9 cc), water saturation (S_w of 0.89 cc), SAS DTRAPW_SAS2 (at 0.8 cc, which represents the foam), and Mg concentration DTRAP_Mg3 (at 0.17 cc, which represents the smart water).

Subsequently, the MORRIS variance-based sensitivity approach results are depicted in Figure 8c. The MORRIS sensitivity analysis plot shows the values of the parameters in accordance with their influence on affecting increased oil recovery profiles. In the MORRIS plot, the parameters farthest to the right on the x-axis represent the most influential parameters on oil recovery profiles during the SWAF-based EOR process. The order of the influence of the parameter is liquid production rate (LigProdCon) as the most impactful, followed by oil saturation (S_o), porosity, water saturation (S_w), SAS (DTRAPW_SAS2) signifying the foam, and Mg concentration (DTRAP_Mg3) denoting the smart water (SW). Thus, based on the MORRIS analysis, the liquid production rate (LigProdCon) exhibited the highest impact on oil recovery profiles.

In summary, combining the results of the three-sensitivity analyses identifies three common characteristics that have the greatest effects on oil recovery: the liquid production rate, foam (DTRAPW SAS2), and Mg (DTRAP Mg3) (LigProdCon). Thus, the three sensitivity analysis approaches show that the relevant parameters are essentially the same in our experiments on the SWAF process. Furthermore, those are the parameters that have the most influence on the incremental oil recovery at core-scale (Hassan *et al.,* 2022a). This suggests that the rate at which the liquid is produced, combined with the SAS and Mg parameters for smart water, significantly impacts incremental oil recovery profiles. Consequently, the SWAF optimization involves utilizing the minimum amount of these parameters (chemicals) for maximum oil recovery. Therefore, the key purpose of these analyses is to minimize the amount of chemicals used while optimizing the recovery with the aid of the gathered insights.

History Matching Process.

As previously mentioned, the history matching process is an optimization process that minimizes the error between the data from the experiments and the simulations. For this study, we have simulated 500 models with different combinations of input parameters to calibrate the simulation model to the experimental coreflooding results (i.e., to reduce the mismatching error of the base case scenario shown earlier in Figure 6b). It is apparent from Figure 6b that the results from the simulation (base case scenario) and the coreflood data do not match. This result shows that the parameters' originally assumed values did not adequately match the actual settings. Further parameter tuning was required to determine their accurate values and achieve a better match. Thus, in the history matching study, we have selected the oil recovery as the objective function to match the simulation data to the coreflood data. The CMG's optimizer DECE and PSO were adopted to generate the different input parameters.

The different models generated by the optimization engine during the history matching are identified by their experimental ID. The model with a set of parameters having the least difference from the experimental results was considered the validated model. The oil recovery profiles for the base case model, the history-matched model, and the experimental data are shown in Figure 9. The latter figure clearly shows the improvement in history matching the coreflooding experimental data using the PSO and DECE optimal history-matched models. In addition, Table 3 provides values for several parameters used in the base-case scenario (assumed) and the history-matched scenario when the optimization software was applied (i.e., PSO and DECE methods). In Table 3, DTRAPW_SAS2 and DTRAP_Mg3 are the relative permeability interpolation parameters for SAS and Magnesium (Mg^{2+}), respectively, K_{RGCL} denotes the relative permeability of the gas phase for the liquid-gas table at connate liquid saturation, K_{ROCW} denotes the oil phase relative permeability for a water-oil table at the connate water saturation, LigProdCon represents the liquid production rate (i.e., 0.2 default value, as shown in Table 2), SORG is the residual oil saturation for the liquid-gas table, and S_o and S_w are the oil and water saturations, respectively.

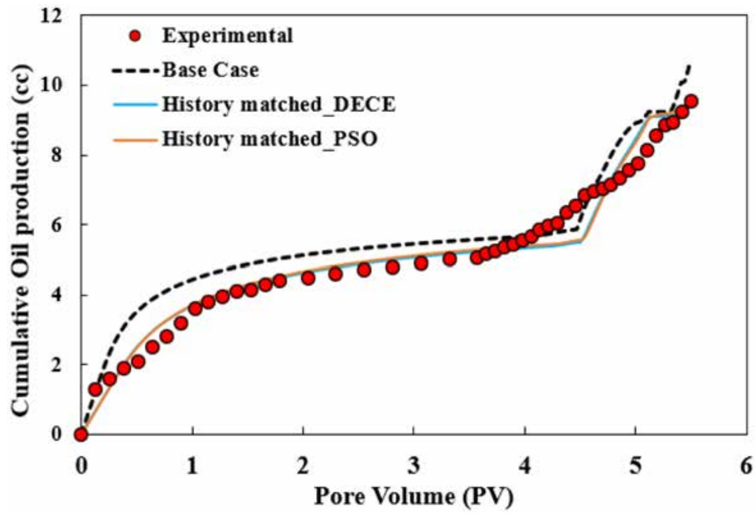

Figure 9—Cumulative oil production (cc) vs. pore volumes (PV) injected from simulation and experimental results.

Table 3—Base-case and history matched-case parameters using the optimization software

Parameters	Base case values	History matched values_DECE	History matched values_PSO
DTRAPW_SAS2	−3	−3.57	−3.6
DTRAP_Mg3	0.000165641	0.000190487	0.000132513
K_{RGCL}	0.8	0.972	0.92
K_{ROCW}	1	0.9075	0.99
LiqProdCon	0.2	0.2015	0.2
Porosity	0.187303586	0.22616958	0.23413
S_{ORG}	0.1	0.10725	0.11
S_o	0.670045	0.6532939	0.6030406
S_w	0.329955	0.48	0.3134572

Figures 10a and 10b exemplify the history matching global error between the simulated and the experimental results for several models with different input settings generated by the DECE and the PSO CMG's optimizers, respectively. Figures 10a and 10b reveal that out of the 500 input value sets, the DECE history-matched parameter values (i.e., optimum solution) and the PSO history-matched parameter values (i.e., optimum solution) have the lowest error between the experimental and the simulated results. The global error of the DECE history-matched optimal solution and the PSO history-matched optimum solution are 4.78% and 4.74%, respectively (i.e., compared to the base case error of 7.94%), as listed in Table 4. It was noted that the PSO method outperformed the DECE one with a slightly lesser global error percentage.

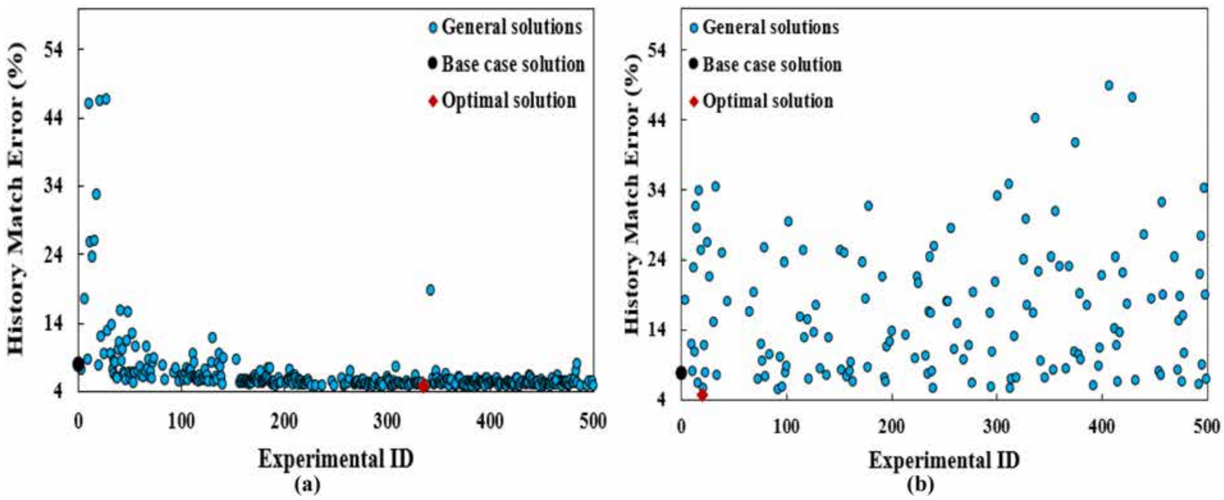

Figure 10—History matching global Error (%) between simulation and experimental data for (a) DECE CMG's optimizer model, and (b) PSO CMG's optimizer model.

Table 4—History matching process results (i.e., global error %) using DECE and PSO CMG's optimizers

Optimization Software -Process	Objective Function	Total Runs	Results		
			Base-Case Global Error	Optimal Global Error (DECE)	Optimal Global Error (PSO)
History Matching	Minimize Global Error (%)	500	7.94 %	4.78 %	4.74 %

Additionally, Figures 11a and 11b display the corresponding water-cut (%) and the oil production (cc) profiles produced from the simulated model results using PSO approach against the coreflooding experimental data. In both figures, the decrease and increase in water-cut and oil production rate observed, respectively at the later part of the injected SWAF flooding (i.e., for both simulated and experimental results) are caused by foam's mobility control.

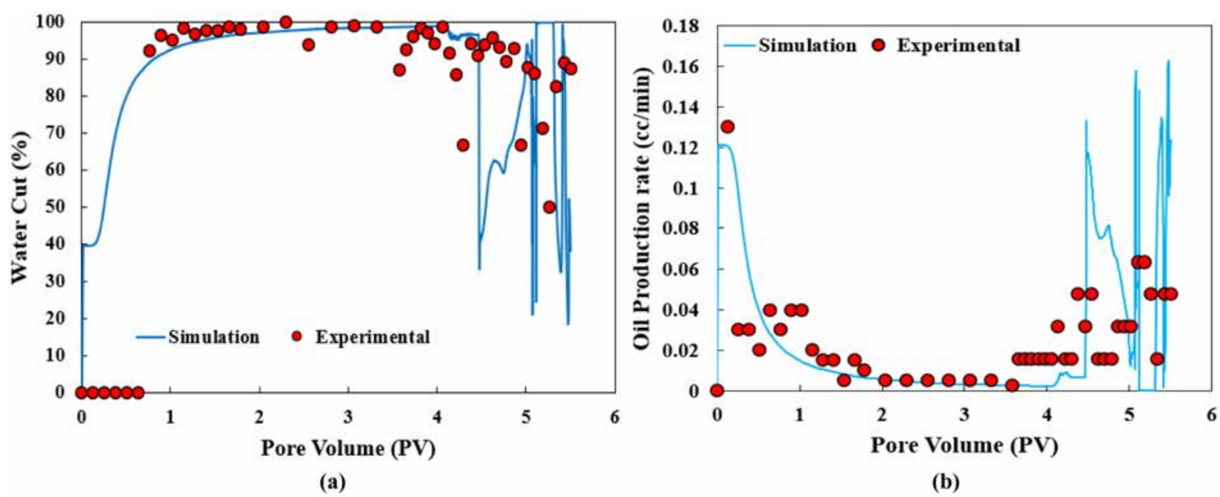

Figure 11—Comparison between simulation and experimental results using PSO approach for (a) Water cut (%) vs. injected PVs, and (b) Oil production rate (cc/min) vs. injected PVs.

Optimization Process.

The objective of the optimization process is to achieve the maximum oil recovery factor with the minimum available chemical concentrations (i.e., Mg^{2+}, SAS, and foam concentrations). For the optimization process, the number of runs utilized is 300. One should note that the initial number of runs selected was 500; however, we extracted the (satisfactory) results after 300 runs. Besides, the optimization process was performed using two different optimization algorithms: DECE and PSO CMG's optimizers.

Regarding the cumulative oil production (cc), Figures 12a and 12b show the optimization process results produced from the DECE and the PSO methods, respectively. The DECE-based optimization process resulted in oil recovery of 9.97 cc, which is higher than the base case recovery of 9.51 (i.e., which exceeds the base case recovery by 0.46 cc), as shown in Figure 12a. Whereas, The PSO-based optimization process resulted in oil recovery of 10.57 cc, which is higher than the base case recovery of 9.51 (i.e., which exceeds the base case recovery by 1.01 cc), as shown in Figure 12b. Figures 13a and 13b show the optimization process results produced from the DECE and the PSO methods, respectively. The DECE-based optimization process resulted in a base case oil recovery of 92.47% and an optimal oil recovery of 96.92%, as shown in Figure 13a. On the other hand, the PSO-based optimization process resulted in a base case oil recovery of 89.49% and optimal oil recovery of 97.92%, as shown in Figure 13b. As a result, we realize that the optimization process based on the PSO method results in a much better-optimized solution. One should also note that the DECE-based optimization process resulted in 5 optimal solutions, which are highlighted in both Figures 13a and 14a. On the other hand, the PSO optimization method resulted in a unique optimal solution for this problem as depicted in Figures 13b and 14b.

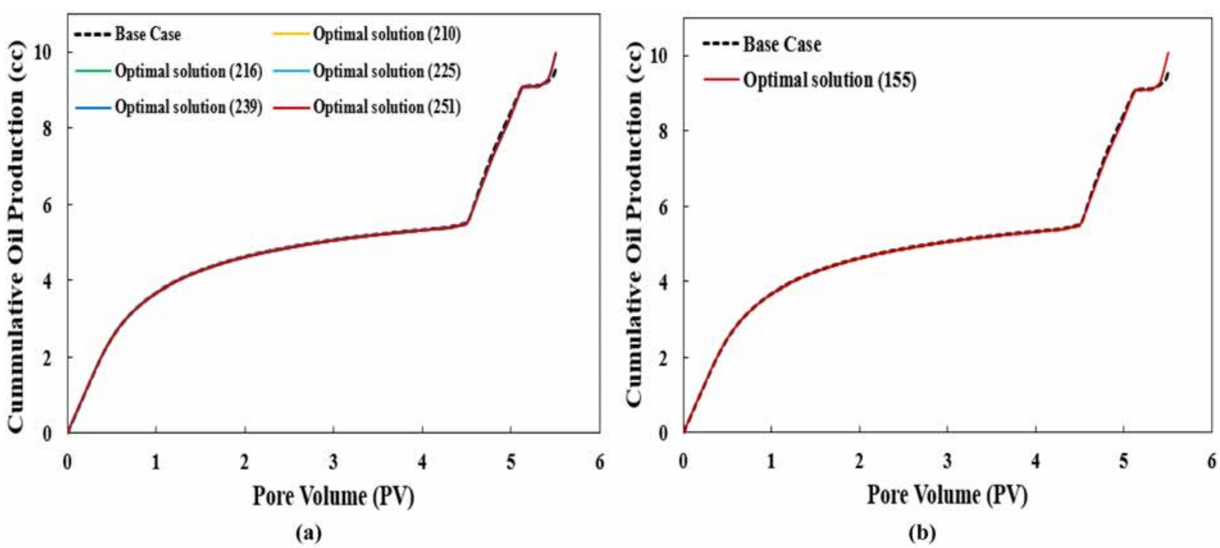

Figure 12—Cumulative oil production profile (cc) vs. injected pore volumes (PV) from optimization process using (a) DECE-based CMG's optimizer, and (b) PSO-based CMG's optimizer.

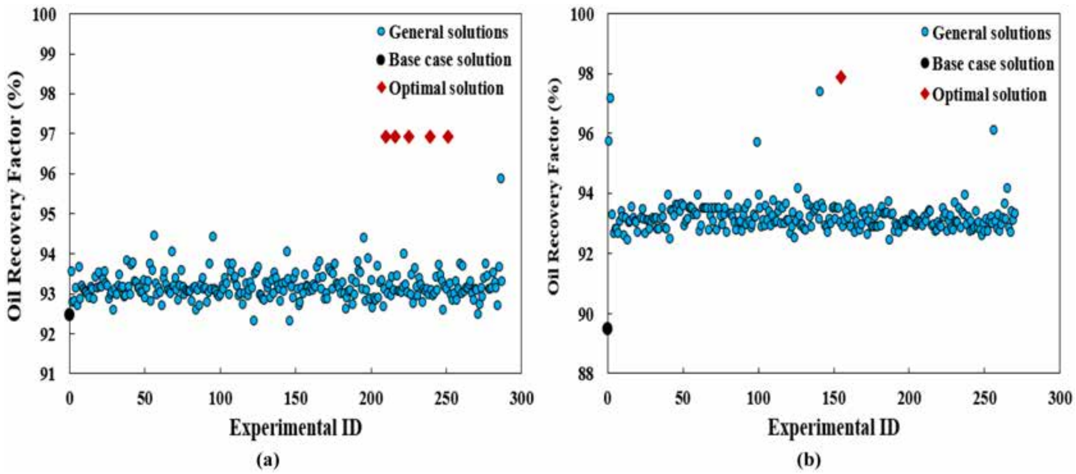

Figure 13—Oil recovery factor (%) vs. injected pore volumes (PV) from the optimization process using (a) DECE-based CMG's optimizer, and (b) PSO-based CMG's optimizer.

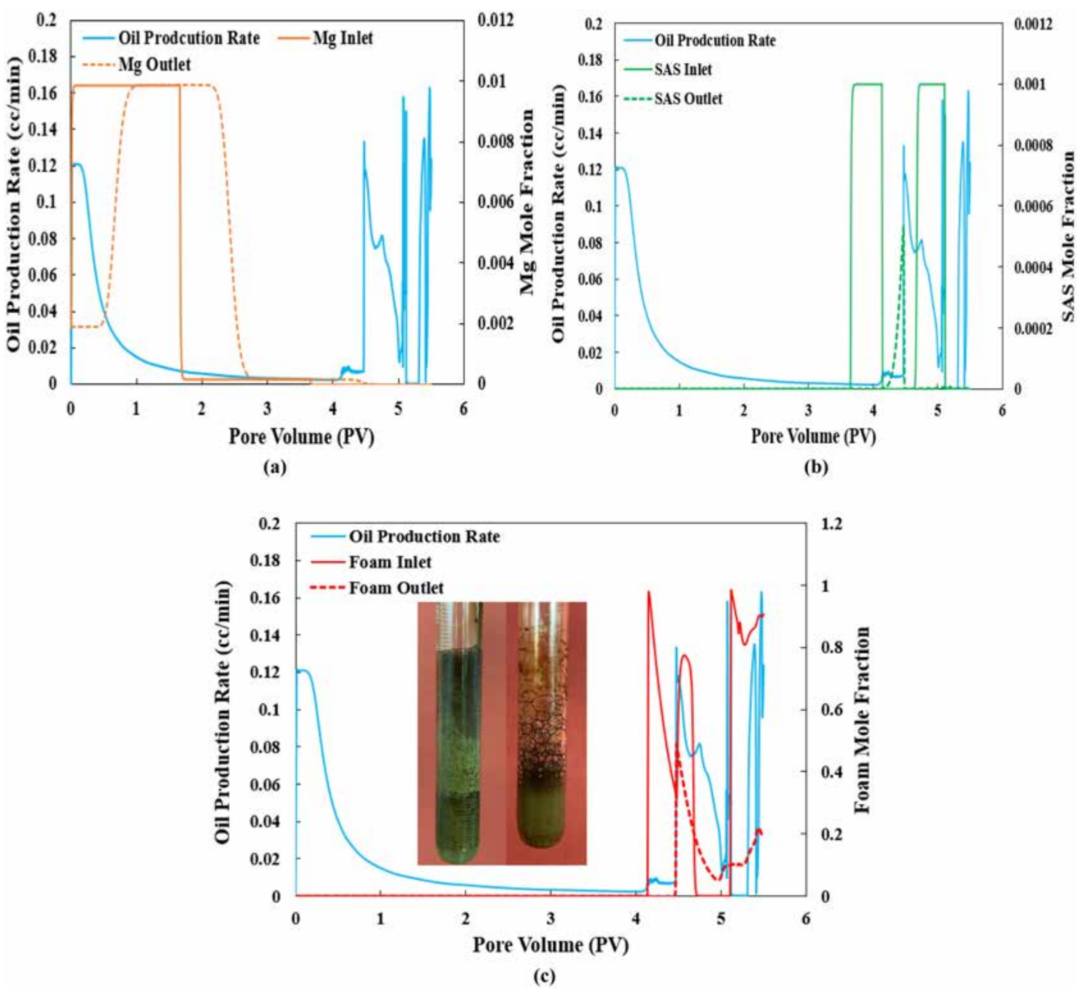

Figure 14—Concentrations of (a) Magnesium-ion, (b) surfactant aqueous solution (SAS), and (c) foam (SAG, SAS alternating gas) at inlet and outlet of history matched simulation model.

Table 5 lists the values of the optimal DECE parameters, Table 6 lists the values of optimal parameters for the PSO-based optimization process, and Table 7 summarizes the oil recovery results (i.e., optimization process) using the DECE and the PSO CMG's optimizers. Overall, it is apparent that in the DECE-based optimal solutions, the chemical concentrations are higher for all three SAS, Foam, and Mg^{2+} as opposed to the PSO optimizer (Tables 5 and 6). In contrast, the oil recovery from the PSO-based optimal solution is clearly higher (Table 7). This infers that, in terms of maximizing oil recovery while minimizing the usage of injected chemicals during SWAF flooding, the optimal solution via the PSO-based approach is superior to the DECE-based optimal solutions.

Table 5—Optimal parameters for DECE obtained during maximizing oil recovery by SWAF flooding

Mole Fractions	Experiment 210	Experiment 216	Experiment 225	Experiment 239	Experiment 251
Foam	0.94	0.9375	0.93375	0.935	0.93625
Mg^{2+}	0.000197206	0.000197206	0.000197206	0.000197206	0.000197206
SAS	0.00076919	0.00076919	0.00076919	0.00076919	0.00076919

Table 6—Optimal parameters for PSO obtained during maximizing oil recovery by SWAF flooding

Mole Fraction	Experiment 155
Foam	0.75295375
Mg^{2+}	0.000179086
SAS	0.000596768

Table 7—Optimization process results (i.e., oil recovery %) using DECE and PSO CMG's optimizers

Optimization Software - Process	Objective Function	Total Runs	Results			
			Base-Case DECE	Optimal DECE	Base-Case PSO	Optimal PSO
Optimization Progress	Maximize Oil Production (%)	300	92.47%	96.92%	89.49%	97.92%

Additionally, Figures 14a, 14b, and 14c show the flows of magnesium (Mg^{2+}) in the explicitly designed smart water (SW), surfactant aqueous solution (SAS), and Foam (SAG), respectively, together with their corresponding impact on oil production. The oil production rate plot at the inlet and outlets of Mg^{2+} (Figure 14a) reveals an exceptionally high preliminary upsurge in the oil production rate until it declines to a virtually insignificant value. The ILS core sample's wettability alteration through smart water is perceived as a minor enhancement in oil recovery (i.e., incremental OIIP of 10%) after injecting smart water. Figure 14b shows that with the flow of the injected SAS towards the outlet, the oil production rate surges. Correspondingly, both the inlet and the outlet exhibited the presence of substantial SAS concentrations that are equivalent to high rates of production at comparable injection PVs at approximately 4 PVs. Additionally, Figure 14c depicts the produced foam at the inlet, where it transmissions across the core before decaying. Consequently, there is a smaller amount of foam at the outlet. Furthermore, the apparent increase in oil production rate is attributed to the SAS induced wettability alteration by foam-assisted mobility control.

Relative Permeability Curves.

This SWAF-based EOR optimization process aims to achieve the optimal solution yielding the maximum oil recovery with minimum chemical expended to render the SWAF process cost-effective. From the previous sensitivity analysis results, we learned that the most influential parameters of improved oil recovery by SWAF-flooding are the liquid production rate (i.e., LiqProdCon), SAS, and Mg^{2+} concentrations in the aqueous solution, which are specified in mole fraction (%), as was previously shown in Figure 14. Subsequently, the relative permeability curves were derived using Corey's correlation; the saturation endpoints of the water-oil table were determined from the results of waterflooding (i.e., seawater, 35000 ppm) (Hassan *et al.,* 2022a). Finally, the effect of wettability alteration by smart water and surfactant solution, and mobility control by foam was incorporated using three sets (i.e., Set-1, Set-2, and Set-3) of relative permeability curves. Table 8 lists the three sets of relative permeability curves with the values of interpolation parameters (i.e., DTRAPW and DTRAPN). DTRAPW (i.e., wetting phase) and DTRAPN (non-wetting phase) are interpolation parameters or tuning parameters used to depict the alteration response to the relative permeability curves.

Table 8—Interpolation parameters (i.e., DTRAPW and DTRAPN)

Interpolation Parameter	Smart Waterflooding (Aqueous Mole Fraction) [Mg]			SAS Flooding (Aqueous Mole Fraction) [SAS]		Foam Flooding (Aqueous Mole Fraction) [Foam]	
	Set 1	Set 2	Set 3	Set 1	Set 2	Set 1	Set 2
DTRAPW	0.00241013	0.00128788	0.000165641	−7	−3	0.0001	0.01
DTRAPN	–	–	–	−7	−3	0.0001	0.01

Figures 15a and 15b illustrate the relative permeability datasets employed for the optimized simulation model using PSO approach. The interpolation sets for the relative permeability of smart waterflooding are shown in Figure 15a. The solid curves denote the seawater (i.e., 35000 ppm) flooding process. In contrast, enhanced relative permeability during the propagation of smart water (i.e., 3500 ppm) flooding is reflected by the dashed curves. This reveals the additional impact of smart water on the relative permeability; although it is moderate (i.e., 10% of the incremental OIIP), the carbonate core sample's wettability is affected by smart water. Further, the interpolation sets of the relative permeability for foam flooding are depicted in Figure 15b. In the latter figure, the seawater flooding process is indicated by solid curves, whereas the dashed curves represent the enhanced relative permeability during foam propagation flooding. It is apparent that a notable increase in oil relative permeability occurs due to the influence of the foam (i.e., wettability alteration and IFT reduction), suggesting the high efficiency of foam injection for wettability alteration in carbonates (i.e., calcite rock), which creates an improved oil production rate (i.e., up to 97.89 % of the OIIP for the optimized model).

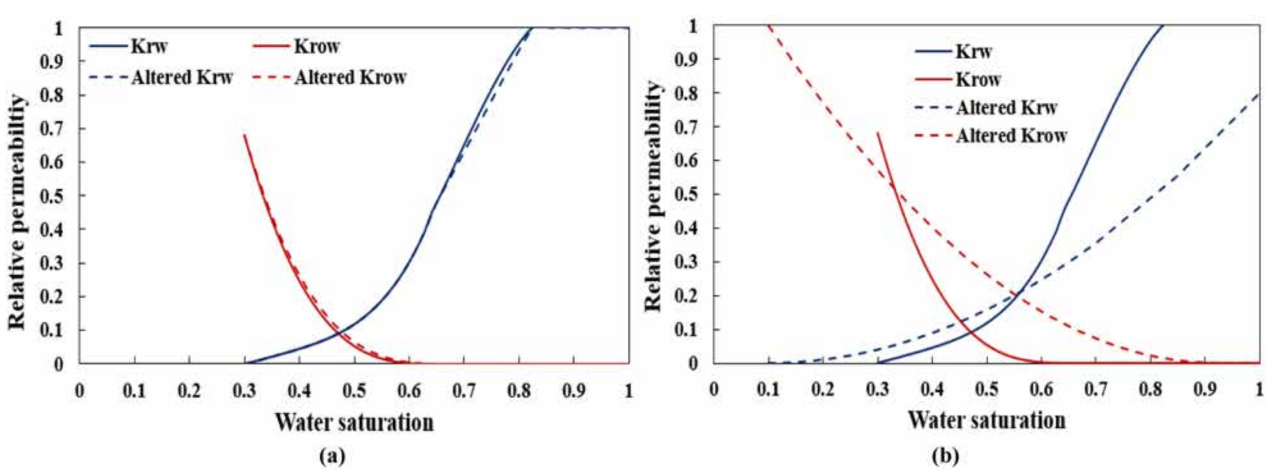

Figure 15—Relative permeability curves used for (a) smart water injection, and (b) foam flooding (i.e., SAS Alternating Gas or SAG).

Summary and Conclusions

This contribution utilizes a core-scale advanced processes reservoir simulation model to provide insights and a better understanding of the governing mechanisms behind incremental oil recovery through a new hybrid

EOR method. This new EOR technology coalesces smart waterflooding and foam injections and is termed Smart Water Assisted Foam (SWAF) flooding, particularly for carbonate reservoirs. This study facilitates the successful field application of SWAF technology in carbonate reservoirs by thoroughly understanding SWAF-oil interactions at reservoir conditions (i.e., 80°C). Hence, the optimization software was used for performing the first important phase of this study, i.e., sensitivity analysis, to determine the impact of various inputs incorporated into the simulation models on the simulation outcomes. The second key stage was history matching, wherein some input parameters (obtained from the sensitivity analysis) were changed to match them with some of the measured coreflood experimental data. Finally, the third essential stage was the optimization process, in which we glanced at varying some of the operational controls for increasing the oil recovery by maximizing the recovery factor, the cumulative oil production rate (cc) or minimizing the cost and environmental impact. The following key findings sum up the results of this numerical study:

- The radial basis function (RBF) neural network proxy model outperforms the polynomial regression in forecasting objective function during the sensitivity analysis study, as evidenced by comparing their respective verification plot.
- Consolidated findings from the three sensitivity analyses, i.e., the Tornado-plot, SOBOL, and MORRIS, outline three common parameters that significantly affect the oil recovery profiles. These are liquid production rate (LigProdCon), foam (DTRAPW SAS2), and Mg^{2+} concentration (DTRAP Mg3) parameters. This suggests that the imperative parameters are virtually the same, whereas during our SWAF experiments at the core-scale, these same imperative parameters had the greatest impact on oil recovery increase (Hassan *et al.,* 2022a).
- The results of the simulated base case using the advanced processes reservoir simulator have a higher history matching error than the optimal solutions using the optimization software. In our situation, the base case error was 7.94 %, while the DECE and PSO-based optimization software techniques showed global errors of 4.78 % and 4.74%, respectively.
- The chemical concentrations in DECE-based optimal solutions are higher for all three SAS, Foam, and Mg^{2+} parameters. On the other hand, the oil recovery from the PSO-based optimal solutions is considerably higher. Thus, in terms of maximizing oil recovery while minimizing the injected chemicals used during the SWAF flooding, the optimal solution via the PSO-based approach is superior (97.89%) to the DECE-based optimal solutions (92.47%).
- The results imply that additional modifications must be made to the optimum chemical injection rate for the SWAF-based EOR flooding scenario to improve the sweep efficiency of carbonate reservoirs.
- This study enables a successful field application of SWAF technology in carbonate reservoirs by thoroughly understanding SWAF-oil interactions at reservoir conditions (i.e., 80°C).

Acknowledgments

The authors would like to extend their appreciation and gratitude to Khalifa University of Science and Technology (Abu Dhabi, UAE) for granting access to their infrastructure. They are also grateful for the generous support given by Universiti Teknologi PETRONAS (UTP), which made this work possible.

Nomenclature: *Symbols*

a_o	Intercept
$a_1, a_2 \ldots \ldots a_k$	Linear terms coefficients
a_{jj}	Quadratic terms coefficients
a_{ij}	Cross (interaction) terms coefficients
K_{rg}	Gas phase relative permeability for liquid-gas table

K_{rgcl} K_{rg} at connate liquid saturation
K_{ro} Oil phase relative permeability
K_{rocw} K_{ro} at connate water saturation
K_{rog} Liquid phase relative permeability for liquid-oil table
K_{rogcg} K_{rog} at connate gas saturation
K_{row} Oil phase relative permeability for water-oil table
K_{rw} Water phase relative permeability for water-oil table
K_{rwiro} K_{rw} at irreducible oil saturation
N_c Capillary number
N_g Exponent for calculating K_{rg} from K_{rgcl}
N_{og} Exponent for calculating K_{rog} from K_{rogcg}
N_{ow} Exponent for calculating K_{row} from K_{rocw}
N_w Exponent for calculating K_{rw} from K_{rwiro}
S_{gcon} Connate gas saturation
S_{gcrit} Critical gas saturation
S_o Oil saturation
S_{oirg} Irreducible oil saturation for liquid-gas table
S_{oirw} Irreducible oil saturation for water-oil table
S_{org} Residual oil saturation for liquid gas table
S_{orw} Residual oil saturation for water-oil table
S_w Water saturation
S_{wcrit} Critical water saturation

Abbreviations

CMG Computer Modelling Group Ltd.
CMG-CMOST Computer Modelling Group's Intelligent Optimization & Analysis Tool
CMG-STARS Computer Modelling Group's Steam, Thermal, and Advanced Processes Simulator
COBR Crude Oil/Brine/Rock
DECE Designed Exploration and Controlled Evolution
DTRAPNA Interpolation parameters low capillary number for high IFT value
DTRAPNB Interpolation parameters high capillary number for ultralow IFT value
EDL Electrical Double Layer
EOR Enhanced Oil Recovery
FAWAG Foam Assisted Water Alternating Gas
FW Formation Water
IFT Interfacial Tension
ILS Indiana Limestone
LigProdCon Liquid Production Rate
OIIP Oil Initial In Place
OPAAT One Parameter At A Time
PSO Particle Swarm Optimization
PVT Pressure, Volume, and Temperature
RBF Radial Basis Function (Reservoir Simulator)
RSM Response Surface Methodology
SAS Surfactant Aqueous Solution
SW Smart Water

SWAF Smart Water Assisted Foam

References

Aarra, M.G., Skauge, A., and Martinsen, H.A., 2002, September. FAWAG: A Breakthrough for EOR in the North Sea. In *SPE annual technical conference and exhibition*. OnePetro.

Akbar, M., Vissapragada, B., Alghamdi, A.H., Allen, D., Herron, M., Carnegie, A., Dutta, D., Olesen, J.R., Chourasiya, R.D., Logan, D., and Stief, D., 2000. A snapshot of carbonate reservoir evaluation. *Oilfield review*, **12** (4), pp.20–21.

Ali, J., Burley, R.W., and Nutt, C.W., 1985. Foam enhanced oil recovery from sand packs. *Chem. Eng. Res. Des.*;(United Kingdom), **63** (2).

Alkhatib, A.M., and King P.R., 2014. The Use of the Least Squares Probabilistic Collocation Method in Decision Making in the Presence of Uncertainty for Chemical EOR Processes. Presented at the SPE Annual Technical Conference and Exhibition, Amsterdam, Netherlands, October. SPE-170587-MS. http://dx.doi.org/10.2118/170587-MS

Al-Shalabi, E.W., Sepehrnoori, K., and Pope, G., 2014. Geochemical investigation of the combined effect of injecting low salinity water and carbon dioxide on carbonate reservoirs. *Energy Procedia*, **63**, pp.7663–7676.

Al-Shalabi, E.W., Sepehrnoori, K., and Pope, G., 2016. Numerical modeling of combined low salinity water and carbon dioxide in carbonate cores. *Journal of Petroleum Science and Engineering*, **137**, pp.157–171.

AlSofi A.M. and Blunt M.J., 2011. The design and optimization of polymer flooding under uncertainty. SPE Enhanced Oil Recovery Conference, Kuala Lumpur, Malaysia, 19-21 July. SPE145110-MS. http://dx.doi.org/10.2118/145110-MS

Alvarado, V. and Manrique, E., 2010. Enhanced oil recovery: an update review. *Energies*, **3** (9), pp.1529–1575.

Bai, G.P. and Xu, Y., 2014. Giant fields retain dominance in reserves growth. *Oil & Gas Journal*, **112** (2), pp.44–44.

Blaker, T., Aarra, M.G., Skauge, A., Rasmussen, L., Celius, H.K., Martinsen, H.A., and Vassenden, F., 2002. Foam for gas mobility control in the Snorre field: the FAWAG project. *SPE Reservoir Evaluation & Engineering*, **5** (4), pp.317–323.

Cheng, X., Kleppe, J., Torsæter, O., 2019. Simulation study of surfactant injection in a fractured core. *J. Pet. Explor. Prod. Technol*. **9**, 3079–3090. https://doi.org/10.1007/s13202-019-0705-y

Computer Modeling Group (CMG), 2019. *User technical manual*.

Corey, A.T., 1977. *Mechanics of heterogeneous fluids in porous media*. Water Resources Publications.

Dalland, M., Hanssen, J.E., and Kristiansen, T.S., 1994. Oil interaction with foams under static and flowing conditions in porous media. *Colloids and Surfaces A: Physicochemical and Engineering Aspects*, **82** (2), pp.129–140.

Denkov, N.D., 2004. Mechanisms of foam destruction by oil-based antifoams. *Langmuir*, **20** (22), pp.9463–9505.

Douarche, F., Da Veiga, S., Feraille, M., Enchéry, G., Touzani, S. and Barsalou, R., 2014. Sensitivity analysis and optimization of surfactant-polymer flooding under uncertainties. *Oil & Gas Science and Technology–Revue d'IFP Energies nouvelles*, **69**(4), pp.603–617.

Dullien, F.A.L., Chatzis, I., and Kantzas, A., 1989. Laboratory studies of macroscopic and microscopic mechanisms of immiscible gas drive-gravity drainage recovery. In *Proceeding of the 3rd International Symposium on Enhanced Oil Recovery*. Maracaibo, Venezuela (Vol. **1**, pp. 424–437).

Espinosa, D., Caldelas, F., Johnston, K., Bryant, S.L., and Huh, C., 2010. Nanoparticle-stabilized supercritical CO_2 foams for potential mobility control applications. In *SPE Improved Oil Recovery Symposium*. OnePetro.

Garcia, D., Arostegui, I. and Prellezo, R., 2019. Robust combination of the Morris and Sobol methods in complex multidimensional models. *Environmental Modelling & Software*, **122**, p.104517.

Garrett, P.R., 2017. The mode of action of antifoams. In *Defoaming* (pp. 1–118). CRC Press.

Hakiki, F., Maharsi, D.A., and Marhaendrajana, T., 2015. Surfactant-polymer coreflood simulation and uncertainty analysis derived from laboratory study. *J. Eng. Technol. Sci.*, **47**, 706–725 https://doi.org/10.5614/j.eng.technol.sci.2015.47.6.9

Hassan, A.M., Ayoub, M., Eissa, M., Al-Shalabi, E.W., Al-Mansour, A., and Al-Quraishi, A., 2022a. Increasing Reservoir Recovery Efficiency through Laboratory-Proven Hybrid Smart Water-Assisted Foam (SWAF) Flooding in Carbonate Reservoirs. *Energies*, **15**(9), p.3058.

Hassan, A.M., Ayoub, M., Eissa, M., Al-Shalabi, E.W., Almansour, A., and Alquraishi, A., 2022c. Foamability and Foam Stability Screening for Smart Water Assisted Foam Flooding: A New Hybrid EOR Method. In *International Petroleum Technology Conference*. OnePetro.

Hassan, A.M., Ayoub, M.A., Mohyaldinn, M.E. and Al-Shalabi, E.W., 2022d, October. Insights into Hybrid Smart Water Assisted Foam (SWAF) Flooding in Carbonate Reservoirs: A Combined Numerical and Experimental Approach. In ADIPEC-2022. OnePetro.

Hassan, A., Ayoub, M., Eissa, M., Bruining, H., Al-Mansour, A., and Al-Guraishi, A., 2020a. A Novel Hybrid Enhanced Oil Recovery Method by Smart Water-Injection and Foam-Flooding in Carbonate Reservoirs. In *SPE/IATMI Asia Pacific Oil & Gas Conference and Exhibition*. OnePetro.

Hassan, A., Ayoub, M., Eissa, M., Bruining, H., Al-Mansour, A., and Al-Guraishi, A., 2020c. A study of combined low salinity foam injection using dlvo theory and surface complexation modeling. In *Offshore Technology Conference Asia*. OnePetro.

Hassan, A., Ayoub, M., Eissa, M., Bruining, H., Al-Mansour, A., and Al-Quraishi, A., 2021. A New Hybrid Improved and Enhanced Oil Recovery IOR/EOR Process Using Smart Water Assisted Foam SWAF Flooding in Carbonate Rocks, A Laboratory Study Approach. In *International Petroleum Technology Conference*. OnePetro.

Hassan, A.M., Ayoub, M., Eissa, M., Bruining, H., and Zitha, P., 2020b. Study of surface complexation modeling on a novel hybrid enhanced oil recovery (EOR) method; smart-water assisted foam-flooding. *Journal of Petroleum Science and Engineering*, **195**, p.107563.

Hassan, A.M., Ayoub, M., Eissa, M., Musa, T., Bruining, H., and Farajzadeh, R., 2019. Exergy return on exergy investment analysis of natural-polymer (Guar-Arabic gum) enhanced oil recovery. *Energy Journal*, **181** (15), pp. 162–172.

Hassan, A.M., Ayoub, M.A., Mohyadinn, M.E., Al-Shalabi, E.W., and Alakbari, F.S., 2022b. A New Insight into Smart Water Assisted Foam SWAF Technology in Carbonate Rocks using Artificial Neural Networks ANNs. In *Offshore Technology Conference Asia*. OnePetro.

Hiorth, A., Cathles, L.M., Kolnes, J., Vikane, O., Lohne, A., and Madland, M.V., 2008. Chemical modeling of wettability change in carbonate rocks. In *10th Wettability Conference*, Abu Dhabi, UAE (pp. 1–9).

Hiorth, A., Cathles, L.M., and Madland, M.V., 2010. The impact of pore water chemistry on carbonate surface charge and oil wettability. *Transport in porous media*, **85** (1), pp.1–21.

Hirasaki, G.J., 1991. Wettability: fundamentals and surface forces. *SPE formation evaluation*, **6** (2), pp.217–226.

Horowitz, B., Guimaraes, L.J., Dantas, V., and Afonso, S.M., 2010. A concurrent efficient global optimization algorithm applied to polymer injection strategies. *J. of Petrol. Sci. and Eng.*, **71** (3): 195–204.

IEA, 2020. *World Energy Outlook*. OECD Publishing.

IEA, 2021. *World Energy Outlook*.

Kuhlman, M.I., 1990. Visualizing the effect of light oil on CO_2 foams. *Journal of petroleum technology*, **42** (7), pp.902–908.

Kumar, A. and Mandal, A., 2020. Core-scale modeling and numerical simulation of zwitterionic surfactant flooding: designing of chemical slug for enhanced oil recovery. *Journal of Petroleum Science and Engineering*, **192**, p.107333.

Lake, L., Johns, R.T., Rossen, W.R., and Pope, G.A., 2014. *Fundamentals of enhanced oil recovery*.

Liu, H. and Chen, Z., 2018. A scalable thermal reservoir simulator for Giant models on parallel computers. arXiv preprint arXiv:1812.03952.

Lunkenheimer, K. and Malysa, K., 2003. Simple and generally applicable method of determination and evaluation of foam properties. *Journal of surfactants and detergents*, **6** (1), pp.69–74.

Masalmeh, S.K., 2012. Impact of capillary forces on residual oil saturation and flooding experiments for mixed to oil-wet carbonate reservoirs. In *SCA* (Vol. **11**, pp. 27–30).

Masalmeh, S.K., Wei, L., and Blom, C.P., 2011. Mobility control for gas injection in heterogeneous carbonate reservoirs: comparison of foams versus polymers. In *SPE Middle East Oil and Gas Show and Conference*. OnePetro.

Morrow, N.R., 1991. *Interfacial phenomena in petroleum recovery*. NR Morrow (ed.), pp.77–99.

Schramm, L.L. and Novosad, J.J., 1992. The destabilization of foams for improved oil recovery by crude oils: Effect of the nature of the oil. *Journal of Petroleum Science and Engineering*, **7** (1-2), pp.77–90.

Schramm, L.L., Turta, A.T., and Novosad, J.J., 1993. Microvisual and coreflood studies of foam interactions with a light crude oil. *SPE reservoir engineering*, **8** (3), pp.201–206.

Simjoo, M., Rezaei, T., Andrianov, A., and Zitha, P.L.J., 2013. Foam stability in the presence of oil: effect of surfactant concentration and oil type. *Colloids and Surfaces A: Physicochemical and Engineering Aspects*, **438**, pp.148–158.

Studart, A.R., Gonzenbach, U.T., Akartuna, I., Tervoort, E., and Gauckler, L.J., 2007. Materials from foams and emulsions stabilized by colloidal particles. *Journal of Materials Chemistry*, **17** (31), pp.3283–3289.

Suarez-Rivera, R., Stenebråten, J., Gadde, P.B., and Sharma, M.M., 2002. An experimental investigation of fracture propagation during water injection. In *International Symposium and Exhibition on Formation Damage Control*. OnePetro.

Taber, J.J., Martin, F.D., and Seright, R.S., 1997. EOR screening criteria revisited Part 1: Introduction to screening criteria and enhanced recovery field projects. *SPE reservoir engineering*, **12** (3), pp. 189–198.

Tunio, S.Q., Chandio, T.A., and Memon, M.K., 2012. Comparative study of FAWAG and SWAG as an effective EOR technique for a Malaysian field. *Research Journal of Applied Sciences, Engineering and Technology*, **4** (6), pp.645–648.

Vikingstad, A.K., Skauge, A., Høiland, H., and Aarra, M., 2005. Foam–oil interactions analyzed by static foam tests. *Colloids and Surfaces A: Physicochemical and Engineering Aspects*, **260** (1-3), pp.189–198.

Weller, A. and Slater, L., 2012. Salinity dependence of complex conductivity of unconsolidated and consolidated materials: Comparisons with electrical double layer models. *Geophysics*, **77** (5), pp. D185–D198.

Xie, Q., Liu, F., Chen, Y., Yang, H., Saeedi, A., and Hossain, M.M., 2019. Effect of electrical double layer and ion exchange on low salinity EOR in a pH-controlled system. *Journal of Petroleum Science and Engineering*, **174**, pp.418–424.

Xue, Z., Worthen, A., Qajar, A., Robert, I., Bryant, S.L., Huh, C., Prodanović, M., and Johnston, K.P., 2016. Viscosity and stability of ultra-high internal phase CO_2-in-water foams stabilized with surfactants and nanoparticles with or without polyelectrolytes. *Journal of colloid and interface science*, **461**, pp.383–395.

Yuncong, G.A.O., Mifu, Z.H.A.O., Jianbo, W.A.N.G., and Chang, Z.O.N.G., 2014. Performance and gas breakthrough during CO_2 immiscible flooding in ultra-low permeability reservoirs. *Petroleum Exploration and Development*, **41** (1), pp.88–95.

Zainal, S., Manap, A.A.A., Hamid, P.A., Othman, M., Chong, M.B.O., Yahaya, A.W., Darman, N.B. and Mat Sai, R., 2008, June. Offshore Chemical EOR: The Role of an Innovative Laboratory Program in Managing Result Uncertainty to Ensure the Success of a Pilot Field Implementation. In Europec/EAGE Conference and Exhibition, Rome, Italy, 9 –12 June. SPE-113154-MS. OnePetro. http://dx.doi.org/10.2118/113154-MS.

Zerpa, L.E., Queipo, N.V., Pintos, S., Tillero, E., and Alter, D., 2007. An efficient response surfaces approach for the optimization of ASP flooding processes: ASP pilot project LL-03 reservoir, SPE Latin America and Caribbean Petroleum Engineering Conference, Buenos Aires, Argentina, 15-18 April. SPE-107847-MS. http://dx.doi.org/10.2118/107847-MS.

Zhang, F., Saputra, I.W., Adel, I.A., and Schechter, D.S., 2019. Numerical Investigation of EOR Applications in Unconventional Liquid Reservoirs through Surfactant-Assisted Spontaneous Imbibition SASI and Gas Injection Following Primary Depletion. In *SPE Annual Technical Conference and Exhibition*. OnePetro.

Appendix A

History Matching Data (PSO: Particle Swarm Optimization)

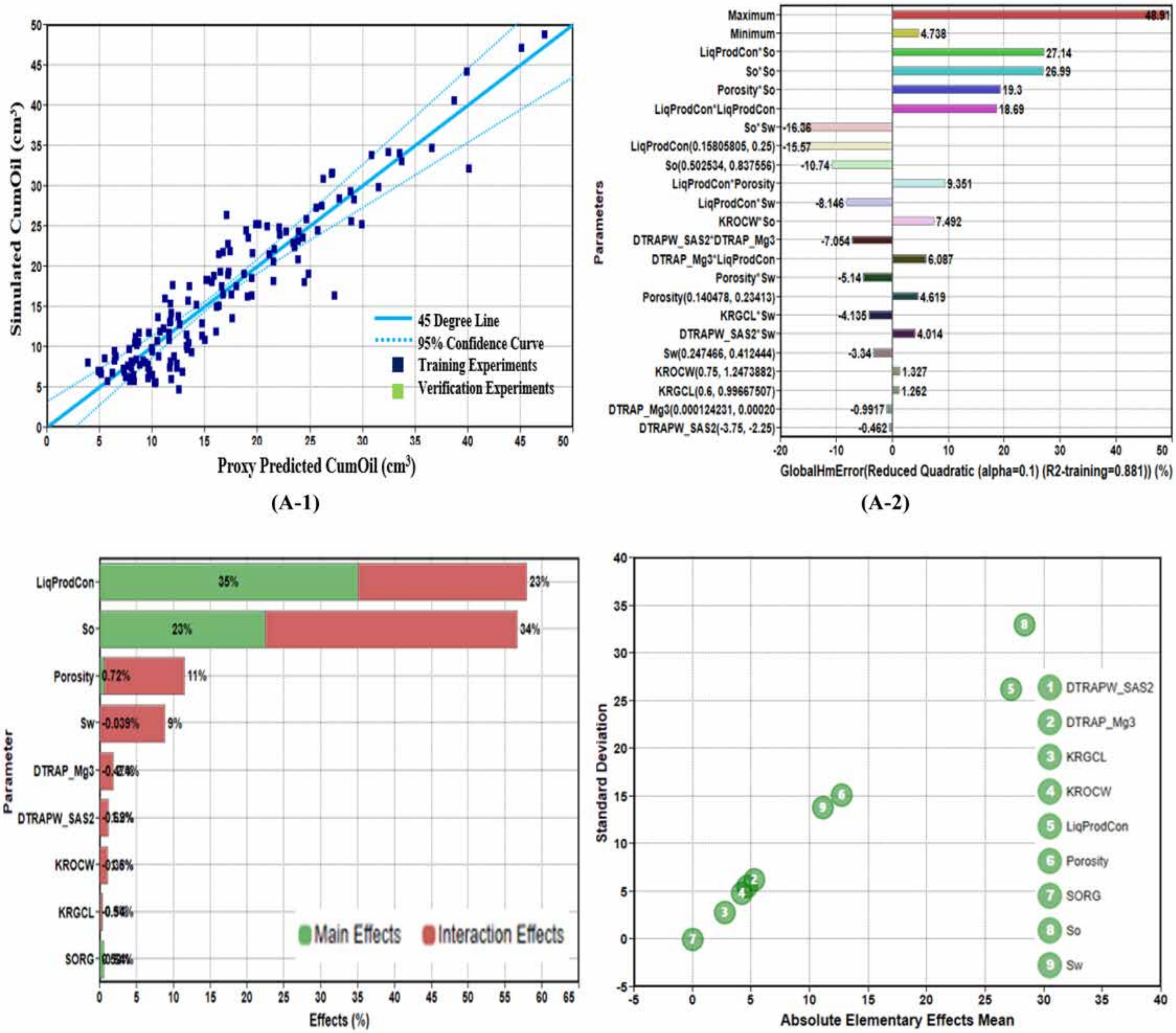

Figure A—PSO-Based history matching data for (A-1) The verification plot analysis used for RPF neural network proxy-model during the history matching study, (A-2) The Tornado plot analysis used for the history matching study, (A-3) The MORRIS analysis used for the history matching study, and (A-4) The SOBOL analysis used for the history matching study.

Objective Function Name: CumOil_Error

Model Classification: Reduced Quadratic (alpha=0.1) (R2-training=0.881)

Table A-1—Summary of fit

R-Square	0.881266
R-Square Adjusted	0.861477

R-Square Prediction	0.828429
Mean of Response	16.3823
Standard Error	3.48148

Table A-2—Analysis of variance

Source	Degrees of Freedom	Sum of Squares	Mean Square	F Ratio	Prob > F
Model	21	11335.2	539.772	44.5332	<0.00001
Error	126	1527.21	12.1207		
Total	147	12862.4			

Table A-3—Effect screening using normalized parameters (-1, +1)

Term	Coefficient	Standard Error	t Ratio	Prob > |t|	VIF
Intercept	9.75437	0.554435	17.5933	<0.00001	0.00
DTRAPW_SAS2(-3.75, −2.25)	−0.231002	0.55395	−0.417008	0.67738	1.30
DTRAP_Mg3(0.000124231, 0.000207051)	−0.495872	0.559557	−0.886187	0.37720	1.49
KRGCL (0.6, 0.99667507)	0.631019	0.520964	1.21125	0.22807	1.25
KROCW (0.75, 1.2473882)	0.663268	0.553916	1.19742	0.23339	1.33
LiqProdCon (0.15805805, 0.25)	−7.78415	0.789001	−9.86583	<0.00001	2.06
Porosity (0.140478, 0.23413)	2.30928	0.740076	3.12033	0.00224	1.51
So (0.502534, 0.837556)	−5.36872	0.682214	−7.86956	<0.00001	1.72
Sw (0.247466, 0.412444)	−1.66998	0.700951	−2.38245	0.01869	1.84
DTRAPW_SAS2*DTRAP_Mg3	−3.52702	0.915267	−3.85354	0.00018	1.32
DTRAPW_SAS2*Sw	2.00707	0.97453	2.05953	0.04150	1.33
DTRAP_Mg3*LiqProdCon	3.04362	0.957196	3.17972	0.00186	1.37
KRGCL*Sw	−2.06752	0.910839	−2.26991	0.02491	1.24
KROCW*So	3.74622	1.02541	3.65339	0.00038	1.50
LiqProdCon*LiqProdCon	9.3452	1.07354	8.70506	<0.00001	1.31
LiqProdCon*Porosity	4.67554	1.47104	3.1784	0.00186	2.07
LiqProdCon*So	13.5687	1.06875	12.6959	<0.00001	1.42
LiqProdCon*Sw	−4.07295	1.15861	−3.51538	0.00061	1.58

Term	Coefficient	Standard Error	t Ratio	Prob > |t|	VIF
Porosity*So	9.65149	1.31527	7.33804	<0.00001	1.70
Porosity*Sw	−2.56992	1.34611	−1.90914	0.05852	1.51
So*So	13.4973	1.01806	13.2578	<0.00001	1.29
So*Sw	−8.18237	1.1236	−7.28231	<0.00001	1.41

Table A-4—Coefficients in terms of actual parameters

Term	Coefficient
Intercept	798.322
DTRAPW_SAS2	7.79855
DTRAP_Mg3	-678874
KRGCL	44.8785
KROCW	-57.5873
LiqProdCon	-3471.67
Porosity	-998.764
So	-1161.05
Sw	918.501
DTRAPW_SAS2*DTRAP_Mg3	-113564
DTRAPW_SAS2*Sw	32.4418
DTRAP_Mg3*LiqProdCon	1.59883E+06
KRGCL*Sw	-126.372
KROCW*So	89.9258
LiqProdCon*LiqProdCon	4422.02
LiqProdCon*Porosity	2172.01
LiqProdCon*So	1762.02
LiqProdCon*Sw	-1074.06
Porosity*So	1230.45
Porosity*Sw	-665.33
So*So	481.018
So*Sw	-592.161

Equation in Terms of Actual Parameters

CumOil_Error=798.322+7.79855*DTRAPW_SAS2-678874*DTRAP_Mg3+44.8785*KRGCL-57.5873*KROCW-3471.67*LiqProdCon-998.764*Porosity-1161.05*So+918.501*Sw-113564*DTRAPW_SAS2*DTRAP_Mg3+32.4418*DTRAPW_SAS2*Sw+1.59883E+06*DTRAP_Mg3*LiqProdCon-126.372*KRGCL*Sw+89.9258 *KROCW*So+4422.02*LiqProdCon*LiqProdCon+2172.01*LiqProdCon*Porosity+1762.02*LiqProdCon*So-1074.06*LiqProdCon*Sw+1230.45*Porosity*So-665.33*Porosity*Sw+481.018*So*So-592.161*So*Sw/

GlobalHmError=798.322+7.79855*DTRAPW_SAS2-678874*DTRAP_Mg3+44.8785*KRGCL-57.5873*KROCW-3471.67*LiqProdCon-998.764*Porosity-1161.05*So+918.501*Sw-113564*DTRAPW_SAS2*DTRAP_Mg3+ 32.4418*DTRAPW_SAS2*Sw+1.59883E+06*DTRAP_Mg3*LiqProdCon-126.372*KRGCL*Sw+89.9258*KROCW*So+4422.02*LiqProdCon*LiqProdCon+2172.01*LiqProdCon*Porosity+1762.02*LiqProdCon*So-1074.06*LiqProdCon*Sw+1230.45*Porosity*So-665.33*Porosity*Sw+481.018*So*So-592.161*So*Sw.

Appendix B

Optimization Progress Data (PSO: Particle Swarm Optimization)

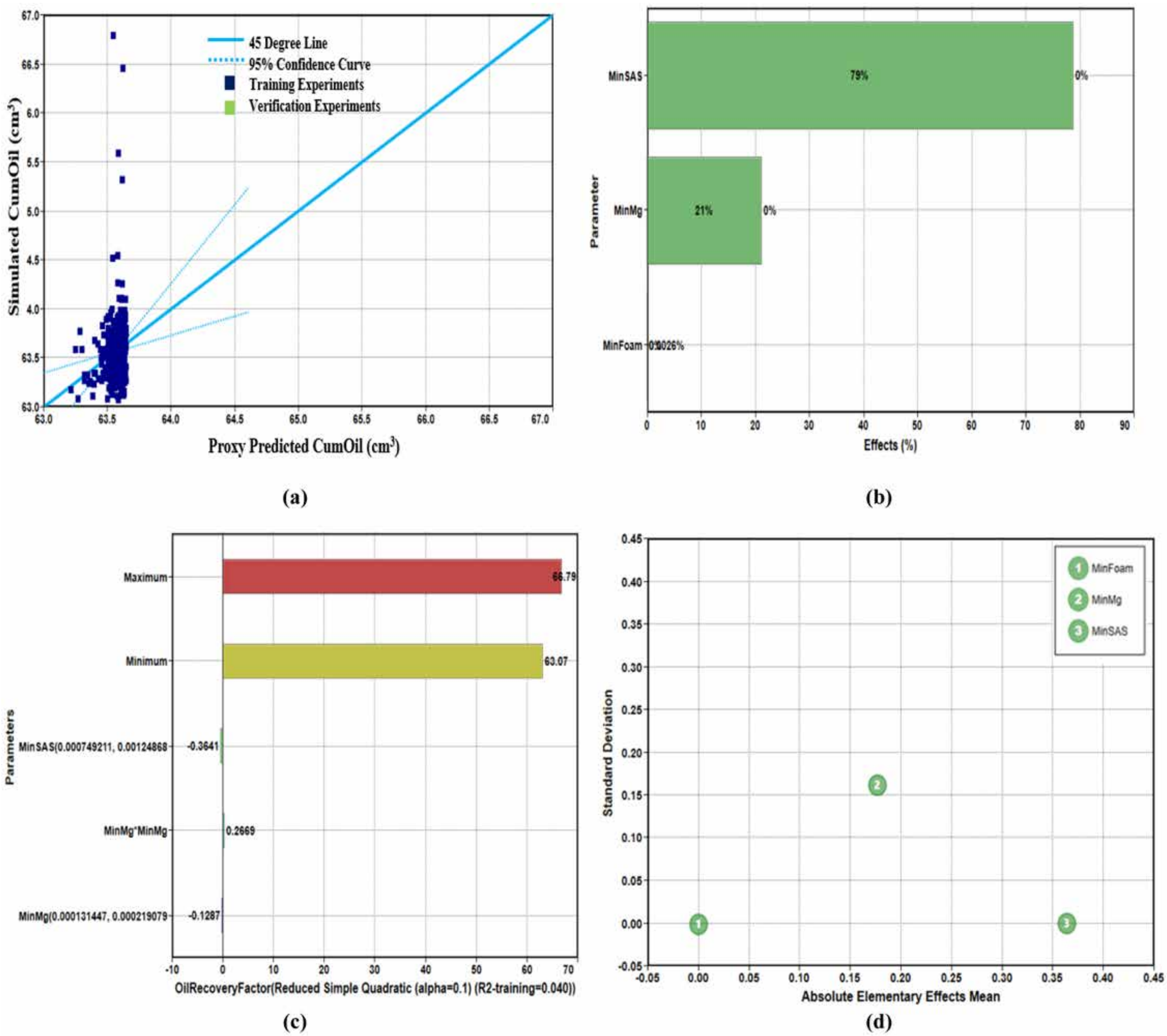

Figure B—PSO-Based optimization process data for (B-1) The verification plot analysis used for RPF neural network proxy-model during the history matching study, (B-2) The Tornado plot analysis used for the history matching study, (B-3) The MORRIS analysis used for the history matching study, and (B-4) The SOBOL analysis used for the history matching study.

Table B5—Summary of fit

R-Square	0.039628
R-Square Adjusted	0.033967
R-Square Prediction	0.027640
Mean of Response	63.5723
Standard Error	0.307412

Table 6—Analysis of variance

Source	Degrees of Freedom	Sum of Squares	Mean Square	F Ratio	Prob > F
Model	3	1.98482	0.661607	7.00095	0.00013
Error	509	48.1017	0.0945024		
Total	512	50.0865			

Table 7—Effect screening using normalized parameters (-1, +1)

Term	Coeficient	Standard Error	t Ratio	Prob > |t|	VIF
Intercept	63.401	0.0405364	1564.05	<0.00001	0.00
MinMg(0.000131447, 0.000219079)	−0.0643303	0.0618373	−1.04032	0.29869	2.73
MinSAS(0.000749211, 0.00124868)	−0.182061	0.050513	−3.60424	0.00034	1.25
MinMg*MinMg	0.133462	0.0606898	2.19909	0.02832	2.35

Table 8—Coefficients in terms of actual parameters

Term	Coefficient
Intercept	66.5219
MinMg	-25835.8
MinSAS	-729.019
MinMg*MinMg	6.95173E+07

Equation in Terms of Actual Parameters

OilRecoveryFactor=66.5219-25835.8*MinMg-729.019*MinSAS+6.95173E+07*MinMg*MinMg